

3D EXPERIMENTAL DETECTION AND DISCRIMINATION OF MALIGNANT AND BENIGN BREAST TUMOR USING NN-BASED UWB IMAGING SYSTEM

S. A. Alshehri

Department of Computer and Communication Systems Engineering
Faculty of Engineering
Universiti Putra Malaysia, Serdang, Selangor 43400, Malaysia

S. Khatun

Department of Computer Systems & Networks
Faculty of Computer Systems & Software Engineering
Universiti Malaysia Pahang
Gambang, Kuantan, Pahang 26300, Malaysia

A. B. Jantan

Department of Computer and Communication Systems Engineering
Faculty of Engineering
Universiti Putra Malaysia, Serdang, Selangor 43400, Malaysia

R. S. A. Raja Abdullah

Wireless & Photonic Networks Research Centre
Universiti Putra Malaysia, Serdang, Selangor 43400, Malaysia

R. Mahmud

Department of Imaging, Faculty of Medicine and Health Sciences
Universiti Putra Malaysia, Serdang, Selangor 43400, Malaysia

Z. Awang

Microwave Technology Center, Faculty of Electrical Engineering
Universiti Teknologi Mara, Shah Alam, Selangor 40400, Malaysia

Abstract—This paper presents both simulation and experimental study to detect and locate breast tumors along with their classification as malignant and/or benign in three dimensional (3D) breast model. The contrast between the dielectric properties of these two tumor types is the main key. These dielectric properties are mainly controlled by the water and blood content of tumors. For simulation, electromagnetic simulator software is used. The experiment is conducted using commercial Ultrawide-Band (UWB) transceivers, Neural Network (NN) based Pattern Recognition (PR) software for imaging and homogenous breast phantom. The 3D homogeneous breast phantom and tumors are fabricated using pure petroleum jelly and a mixture of wheat flour and water respectively. The simulation and experimental setups are performed by transmitting the UWB signals from one side of the breast model and receiving from opposite side diagonally. Using discrete cosine transform (DCT) of received signals, we have trained and tested the developed experimental Neural Network model. In 3D breast model, the achieved detection accuracy of tumor existence is around 100%, while the locating accuracy in terms of (x, y, z) position of a tumor within the breast reached approximately 89.2% and 86.6% in simulation and experimental works respectively. For classification, the permittivity and conductivity detection accuracy are 98.0% and 99.1% in simulation, and 98.6% and 99.5% in experimental works respectively. Tumor detection and type specification 3D may lead to successful clinical implementation followed by saving of precious human lives in the near future.

1. INTRODUCTION

There are many reported simulation and experimental studies on breast tumor detection using Ultrawide-Band (UWB) imaging. Several successful works have been conducted based on numerical breast model [1–8]. Some accomplished experimental works are presented in [9–14]. Many of those are based on the Confocal Microwave Imaging (CMI) approach which depends on the prior knowledge of breast tissue permittivity. This tissue permittivity is obtainable in simulation and experimental works but difficult to be known clinically due to glandular nature of breast tissue and its permittivity variation depending on certain constrains. This may lead to difficulty for such approaches to be implemented clinically [15]. To overcome these problems, we introduce a new non-confocal approach for possible easy clinical implementation [15]. We are presently in the process to obtain Ethical Committee approval to start the clinical trial. This method was based on performing Neural Network (NN) training in one dimension

(1D). The detection in two dimensions (2D) and three dimensions (3D) was done by rotating the transmitter and receiver pair (TX-RX) 360° around the breast model [6].

The main principle in UWB imaging application is the use of contrast in dielectric properties among different breast tissues [10, 16]. If a tumor is detected in a patient's breast, the next importance to the physicians to know its specific type. There are two main types of tumor, namely, malignant and benign [17]. Usually, malignant tumor is known as cancer and a deadly disease while a benign one is not always harmful. Most of the current breast cancer detection methods are unable to differentiate between these two types. It is important to take immediate medical action if the detected tumor is malignant.

There are several indicators to distinguish between benign and malignant tumors, such as shape, size, and stiffness [9, 18, 19]. Tumor viscosity is another important factor [16]. A malignant tumor is more viscous than benign one. The dielectric properties (such as permittivity, density, conductivity, etc.) of malignant tumors are higher because of their higher water and blood contents [17, 18, 20, 21].

At the center frequency of 4.7 GHz: about (i) 67% of benign tumors have a dielectric constant less than or equal to 50; (ii) 10% are greater than 55; and (iii) the rest are in between 50 to 55 [17]. Also at the same frequency around, (iv) 70% of the malignant tumors have dielectric constants greater than 70 and (v) 25% is less than 50. This shows a narrow margin for the dielectric constant values between 50 and 55. Tissues with higher dielectric constants produce more scattered signal than tissues with lower dielectric constants for incident UWB signals [9, 17].

Some researches have been done to classify the tumor types [9, 19, 20, 22]. The classification was based on either (i) their shape or (ii) the use of ultrasonic waves. But, the results could not be obtained in a very early stage of tumor. O'Halloran et al. presented the use of Spiking Neural Networks (SNN) to distinguish between malignant and benign tumors [23]. In our study, we elaborate their concept using Neural Network (NN) based Ultra Wide Band (UWB) system to measure the dielectric values and then to distinguish between malignant and benign tumors accordingly in 3D breast model. Detection of tumor dielectric properties correctly provides better basis for the tumor classification.

In this paper, we employ NN-based UWB approach to detect tumor existence with classification. For this 3D system, no TX-RX rotation is required. This may make clinical implementation easier followed by user friendly regular breast monitoring system, which could be used by end users or patients at home. It also presents the possibility

of distinguishing between malignant and benign tumors based on their dielectric properties. The breast model and phantom used in this study are homogenous. The expected difference between homogenous and heterogeneous breast phantoms was presented in [15].

The paper is organized as follows. The next section presents simulation and experimental tumor detection process details in 3D, followed by tumor type specification, the results and finally the conclusion.

2. METHOD

The high contrast in dielectric properties between normal breast tissues and tumor tissues is the principle behind breast cancer detection using UWB imaging [17]. It is not important to know the exact dielectric values while the ratio between them is important [22, 24]. The ratio of tumor to adipose breast tissue dielectric properties can be 10 : 1, while it could be low as 1.1 : 1 for glandular breast tissue [17].

Here, the considered 3D breast model is similar to the breast model presented in [15] in size (diameter \sim 100 mm, height \sim 50 mm, and skin thickness \sim 2 mm) and shape but prone position. It has similar dielectric properties at center frequency 4.7 GHz [15].

2.1. Neural Network Model and Data Collection

Throughout this research work, the used NN models were back-propagation feed-forward built in MatLab. Table 1 shows the common NN parameters.

To generate the UWB signals for simulation work, we have used the following steps [6]:

- 1) Place a transmitter-receiver pair at opposite sides of the breast model.
- 2) Place a tumor at any locations in the breast model.
- 3) Transmit 4.7 GHz (center frequency) signal using a plane wave located in the x -axis direction.
- 4) Receive the forward scattered signal from the opposite side of breast using software probe.
- 5) Change the tumor location and repeat steps 2–4 several times.

To generate the feature vector for NN training and testing (which are constructed from the received UWB signals amplitudes in time domain), we have used the following steps [6]:

- 1) Interpolate the received signals using “shape-preserving piecewise cubic interpolation” to generate 751 fixed time steps.

Table 1. *NN* parameters.

| <i>NN</i> parameters used in MATLAB | <i>NN</i> for simulation | <i>NN</i> for experiments |
|-------------------------------------|---|--|
| Number of nodes in Input layer | 751 | 251 |
| Number of nodes in Hidden layer | 3 | 3 |
| Number of nodes in Output layer | <ul style="list-style-type: none"> • 3 (for 3D tumor localization) • 2 (for dielectric property estimation) | <ul style="list-style-type: none"> • 3 (for 3D tumor localization) • 2 (for dielectric property estimation) |
| Transfer function | tansig | tansig |
| Training function | traingdm | traingdm |
| Learning rate | 0.005 | 0.005 |
| Momentum constant | 0.6 | 0.6 |
| Maximum number of Epochs | 400000 | 400000 |
| Minimum performance gradient | 1e-25 | 1e-25 |

- 2) Insert the received signals to *NN* with and without the presence of tumor in the breast model.
- 3) Shuffle the signal order in the feature vector for *NN* generalizing purposes.
- 4) Generate the target vector dividing by the diameter of breast to limit the output values to be less than 1. This is because the used transfer function “tansig” has output in the range of $[-1, +1]$.

Once this feature vector is generated, the data is divided into three groups as: (i) training, (ii) validating and (iii) testing.

For the experimental work, we followed the same procedures except that the received signals were transformed into frequency domain using Discrete Cosine Transform (DCT) [15]. The target values for both simulation and experimental works are presented in the following respective sections.

2.2. Tumor Detection in 3D

2.2.1. Simulation Work

CST electromagnetic simulator software is used to construct the simulation environment [25]. The breast model is divided into four layers. Each group of tumors are placed in each specific layer, the probe is placed on same level at the opposite side of transmitter. Some of the tumor positions in each layer are shown in Figure 1. Figure 2 shows the tumor locations in Layers 1 and 3. We have generated a

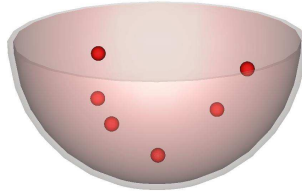


Figure 1. Breast and some tumor models in CST software.

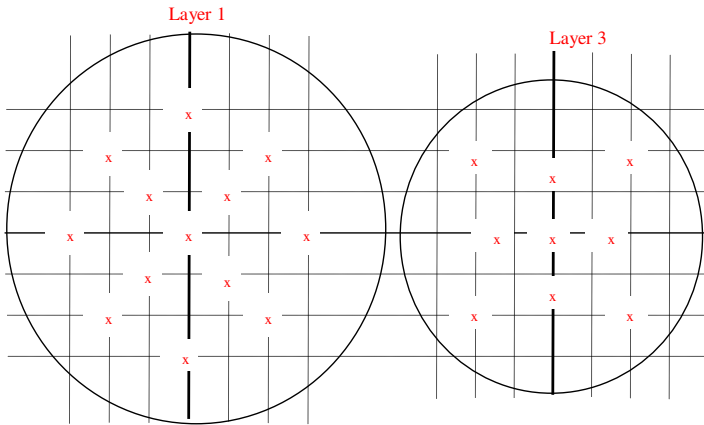


Figure 2. Top view of Layers 1 and 3 tumor positions. The dimensions are in 10 mm increments.

total number of 44 UWB signals (among those, 36 with, and 8 without the presence of tumor). Then the signals are divided into three groups as follows:

- (i) 22 signals for training,
- (ii) 11 for validation and
- (iii) 11 for testing.

The NN output is the tumor (x, y, z) location in 3D. For tumor absence, the x, y and z values are coded as (-1) .

2.2.2. Detection in Experimental Setup

The experimental setup and breast phantom used in [15] is also utilized here. Pure petroleum jelly is used to mimic the breast fatty tissue because of ease of manipulation. The dielectric property measurements of materials is done using Agilent N5230A VNA and HP 85070B dielectric coaxial probe. Figure 3 shows the experimental system setup.



Figure 3. Experimental system setup scenario.



Figure 4. Opened wooden ball that holds the tumor.

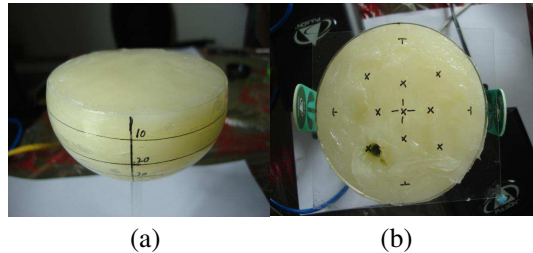


Figure 5. Breast phantom (a) divided into four layers, (b) tumor positions in Layer 3.

The UWB transmitter (TX) and receiver (RX) are connected to a PC using an Ethernet hub and can be controlled through the PC.

A PulsOn UWB transmitter and receiver have been used to transmit and receive the desired UWB signals. This device operates at a center frequency 4.7 GHz and with a 3.2 GHz bandwidth [26]. It uses omnidirectional antenna, also we have developed and used UWB directional antenna for better detection performance.

The experimental work procedure is similar to simulation, presented in the Section 2.1. We have used the same homogeneous breast phantom presented in [15]. Figure 4 shows how the easy way to insert a tumor in the breast phantom. It is inserted inside a wooden ball. The figure presents an opened ball to show the tumor inside it. The wood has permittivity similar to that of the petroleum jelly [27]. Figure 5 shows how the breast phantom is divided into layers to obtain 3D representation. It also shows the top view tumor positions in Layer 3.

Figure 6 shows the waveform of two received UWB signals and their calculated Discrete Cosine Transform (DCT) components. Both of the signals contains tumors signature in two different locations.

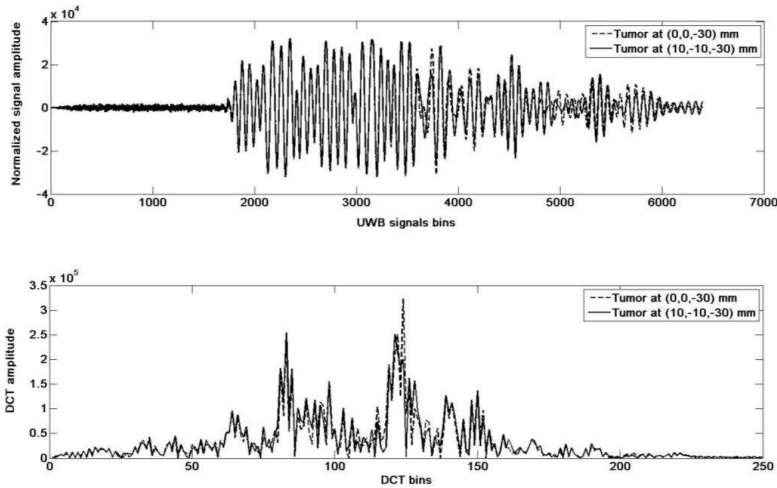


Figure 6. Raw and DCT of two UWB received signals with embedded tumors.

2.3. Discrimination between Malignant and Benign

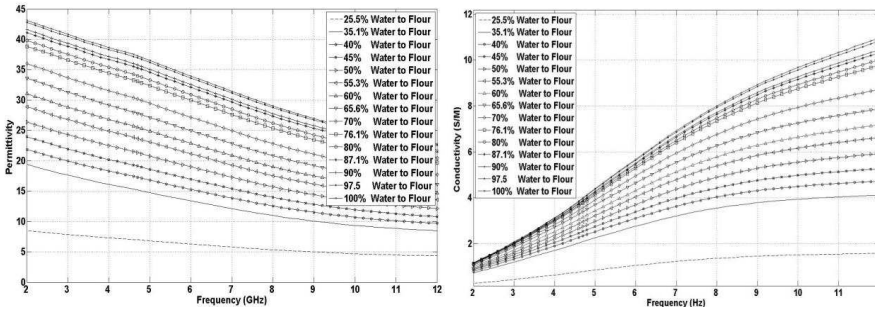
2.3.1. Discrimination in Simulation Setup

The simulation is done using CST EM simulation software by placing a 2.5-mm tumor at $(x = 0, y = 0, z = -0.4)$ mm and varying its dielectric properties. For each value, a UWB signal is transmitted and the propagated signal is received on the opposite side. The collection of received signals is used to construct the feature vector for NN training.

2.3.2. Experimental Work

The same procedure presented in Section 2.1 is followed here. Figure 7 shows the measured permittivity and calculated conductivity for different water-to-flour ratios in the range of 2–12 GHz. Signals corresponding to various dielectric properties values are generated to train the NN. We have used different ratios of water to wheat flour to form the tumor with different dielectric properties as shown in Table 2. Signals for 14 various dielectric values were generated repeatedly three times for each to generate a total number of 42 signals. The signals were divided into three groups as:

- (i) 26 signals for training,
- (ii) 8 for validation and
- (iii) 8 for testing.



(a) Permittivity

(b) conductivity

Figure 7. Constructed tumors using various water-to-flour ratios.

Table 2. Dielectric properties of the used materials at 4.7 GHz.

| Breast phantom part | MATERIAL | Permittivity | Conductivity (S/M) |
|---------------------|------------------------------|--------------|--------------------|
| Fatty breast tissue | Vaseline | 2.36 | 0.012 |
| Tumor | Various water to flour ratio | 15.2–37.3 | 2.1–4.0 |
| Skin | Glass | 3.5–10 | negligible |

In this experimental setup, we first placed a 5-mm (diameter) tumor with the lowest possible dielectric constant value at a distance 50 mm along the line of sight between the transmitter and receiver. After that, the UWB signal was transmitted from one side and received on the other side. Finally, the water-to-flour ratio was varied 14 times to generate different dielectric properties values. The tumor size and location were kept constant.

A Discrete Cosine Transform (DCT) is applied to all of the collected UWB signals. The DCT values between 50 and 300 are used to generate the training feature vector. This is because the transform shows higher values in this interval.

Measuring the NN model performance can be done using several methods. In case of classification application (tumor existence detection), the straightforward and most widely used method is counting the number of missed classifications when the NN is subject to hold-out (test) samples. In the regression case (tumor location, dielectric property estimation), the absolute error is calculated and averaged over the test data size using Equation (1).

$$E = \frac{1}{N} \sum_n (t_n - y_n) \tag{1}$$

where t_n and y_n are the true and NN predicted values for the n th target respectively. N is the hold-out (test) data size. For example, in case of predicting the tumor permittivity, t_n is the actual permittivity of the test data and y_n is the permittivity produced by the NN.

3. RESULTS

3.1. Detection and Localization in 3D

The simulation and experimental 3D location performance accuracies are around 89.2% and 86.6% respectively. The detection rate is almost 100% based on the NN output value. If the NN output has a large negative value (< -0.9) then the tumor does not exist. Here, the tumor locating performance is 7.7% lower than the value reported in [15] because of the fixed TX-RX position and the limited number of training examples. Even though this produced less performance accuracy, it may facilitate the easy clinical implementation. Figure 8 shows some tumors actual and predicted positions. The white balls represent the NN output.

3.2. Discrimination between Malignant and Benign

Table 5 shows simulation and experimental results for some of the dielectric properties values used for NN training, validation and testing. The experimental work shows accuracy in predicting tumor permittivity and conductivity approximately 98.6% and 99.5% respectively.

In the experimental work, it was difficult to generate many water-to-flour ratio values. This limits the number of training samples, which is an important factor in successful NN. However, the detection capability of this proposed system can be used to estimate the viscosity of the existing tumor. As there is no sharp boundary in the dielectric properties values between malignant and benign tumors, the viscosity

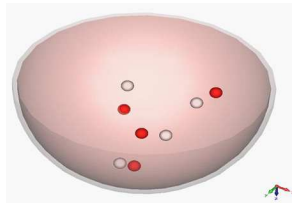


Figure 8. Actual (red) and predicted (white) positions of some tumors.

Table 3. 3D locations of actual and predicted (simulation result as NN output) tumors in simulation work.

| Simulation | | | | | |
|-----------------|------|-----|-----------|--------|--------|
| Actual location | | | NN output | | |
| x | y | z | x | y | z |
| 0.5 | 0.7 | 0.4 | 0.496 | 0.656 | 0.634 |
| -1 | -1 | -1 | -0.999 | -0.991 | -0.994 |
| -1 | -1 | -1 | -0.999 | -0.991 | -0.994 |
| 0.4 | 0.4 | 0.2 | 0.433 | 0.164 | 0.267 |
| 0.5 | 0.3 | 0.4 | 0.561 | 0.409 | 0.420 |
| 0.3 | 0.7 | 0.6 | 0.404 | 0.269 | 0.316 |
| 0.6 | 0.4 | 0.2 | 0.511 | 0.303 | 0.329 |
| 0.5 | 0.5 | 0.2 | 0.517 | 0.499 | 0.409 |
| 0.3 | 0.3 | 0.2 | 0.491 | 0.313 | 0.379 |
| 0.5 | 0.8 | 0.2 | 0.575 | 0.648 | 0.609 |
| 0.6 | 0.6 | 0.2 | 0.432 | 0.642 | 0.409 |
| 0.65 | 0.8 | 0.4 | 0.551 | 0.738 | 0.574 |
| 0.35 | 0.5 | 0.6 | 0.456 | 0.479 | 0.426 |
| 0.5 | 0.5 | 0.6 | 0.618 | 0.506 | 0.506 |
| 0.8 | 0.35 | 0.4 | 0.652 | 0.319 | 0.577 |
| 0.7 | 0.5 | 0.4 | 0.637 | 0.560 | 0.591 |
| 0.32 | 0.65 | 0.8 | 0.403 | 0.601 | 0.421 |
| 0.3 | 0.7 | 0.2 | 0.383 | 0.584 | 0.473 |
| 0.3 | 0.3 | 0.8 | 0.310 | 0.297 | 0.493 |
| 0.7 | 0.3 | 0.2 | 0.621 | 0.302 | 0.404 |
| -1 | -1 | -1 | -0.999 | -0.991 | -0.994 |
| 0.7 | 0.3 | 0.6 | 0.640 | 0.505 | 0.668 |

Since the transfer function “tansig” used in NN training has output in the range $[-1, +1]$, we coded (x, y, z) values to match this range. $(x, y, z) = ((X + 50)/100, (Y + 50)/100, -Z/50)$, where (X, Y, Z) is the original location in the 3D breast model. $(x, y, z) = (-1, -1, -1)$ means tumor does not exist (or healthy breast).

could be taken into account to narrow down the contrast region ($50 < \text{permittivity} < 55$) and sharpen the boundary for tumor type detection. After that it is up to the physician to make the final decision about tumor type and take further medical steps.

Figures 9 and 10 show comparisons between some actual and predicted permittivity and conductivity values in simulation and

Table 4. 3D locations of actual and predicted (experimental result as NN output) tumors in experimental work.

| Experiment | | | | | |
|------------------|-------|------|-----------|--------|--------|
| Actual locations | | | NN output | | |
| x | y | z | x | y | z |
| -0.3 | 0.15 | -0.2 | -0.051 | -0.040 | -0.214 |
| 0 | 0 | -0.4 | 0.096 | 0.035 | -0.343 |
| 0.15 | 0.3 | -0.2 | -0.623 | -0.719 | -0.680 |
| 0 | 0.2 | -0.2 | -0.051 | -0.040 | -0.214 |
| 0.1 | 0.1 | -0.1 | -0.051 | -0.040 | -0.214 |
| -1 | -1 | -1 | -0.967 | -0.989 | -0.965 |
| 0.2 | -0.2 | -0.1 | -0.051 | -0.040 | -0.214 |
| 0.2 | 0.2 | -0.3 | 0.093 | 0.032 | -0.345 |
| 0 | 0.2 | -0.2 | -0.051 | -0.040 | -0.214 |
| 0 | -0.15 | -0.3 | -0.051 | -0.040 | -0.214 |
| 0.1 | -0.1 | -0.1 | -0.051 | -0.040 | -0.214 |
| -0.15 | 0 | -0.3 | -0.051 | -0.040 | -0.214 |
| 0.2 | -0.2 | -0.3 | -0.051 | -0.040 | -0.214 |
| 0 | -0.15 | -0.3 | -0.051 | -0.040 | -0.214 |
| -1 | -1 | -1 | -0.966 | -0.988 | -0.964 |
| -0.2 | -0.2 | -0.4 | 0.049 | -0.023 | -0.375 |
| 0.2 | -0.2 | -0.1 | -0.051 | -0.040 | -0.214 |
| -0.1 | 0.1 | -0.1 | -0.051 | -0.040 | -0.214 |
| -0.1 | 0.1 | -0.1 | -0.051 | -0.040 | -0.214 |
| 0 | 0 | -0.1 | -0.051 | -0.040 | -0.214 |
| 0.18 | 0.2 | -0.4 | 0.066 | -0.002 | -0.364 |
| 0 | 0 | -0.1 | -0.051 | -0.040 | -0.214 |

Since the transfer function “tansig” used in NN training has output in the range $[-1, +1]$, we coded (x, y, z) values to match this range. $(x, y, z) = ((X + 50)/100, (Y + 50)/100, -Z/50)$, where (X, Y, Z) is the original location in the 3D breast model. $(x, y, z) = (-1, -1, -1)$ means tumor does not exist (or healthy breast).

experimental work. They agree very well and reside on the diagonal line indicating the efficiency of the NN model and the system.

In Figure 11, some permittivity values of test group tumors are shown. The permittivity values are shown inside each corresponding tumor object. So, if the tumor permittivity is less than 50, the decision would be that the tumor is benign. If the value is greater than 55 then

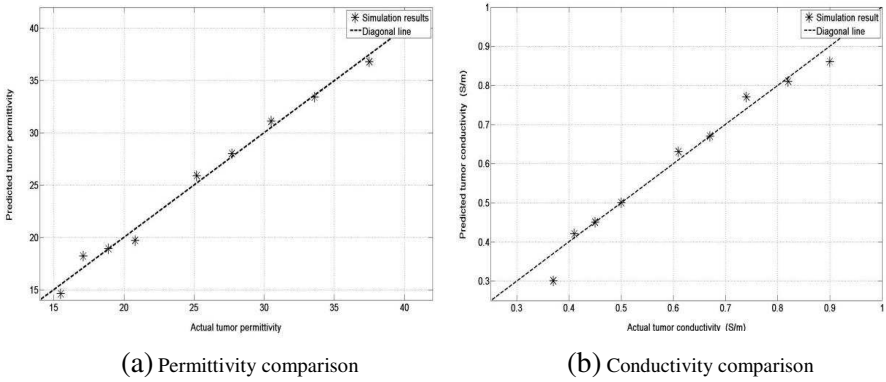


Figure 9. Actual and predicted dielectric property comparison in simulation work.

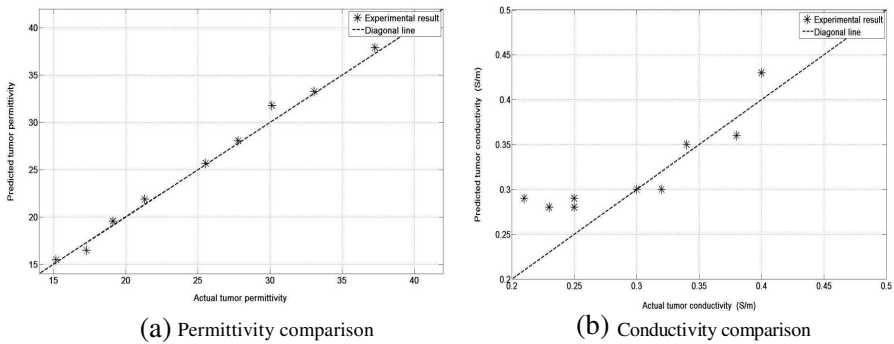


Figure 10. Actual and predicted dielectric property comparison in experimental work.

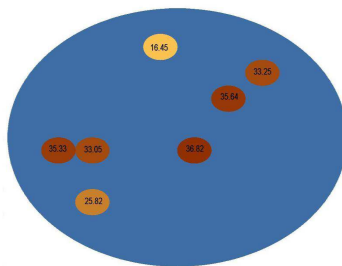


Figure 11. Permittivity value (NN output) of some of the validating and test groups.

Table 5. Tumor dielectric properties found experimentally and in simulation.

| Groups | Simulation | | | | Experiment | | | |
|----------|--------------|-----------|--------------------|-----------|--------------|-----------|--------------------|-----------|
| | Permittivity | | Conductivity (S/m) | | Permittivity | | Conductivity (S/m) | |
| | Actual | NN output | Actual | NN output | Actual | NN output | Actual | NN output |
| Train | 7.9 | 8.0 | 1.8 | 2.4 | 15.18 | 15.45 | 2.1 | 2.9 |
| | 9.6 | 10.0 | 2.2 | 2.5 | 19.12 | 19.56 | 2.5 | 2.9 |
| | 10.6 | 10.7 | 2.4 | 2.6 | 21.33 | 21.87 | 2.5 | 2.8 |
| | 11.6 | 13.4 | 2.7 | 2.7 | 23.68 | 23.97 | 2.7 | 3.0 |
| | 12.8 | 11.3 | 3.0 | 2.8 | 25.54 | 25.66 | 3.0 | 3.0 |
| | 15.5 | 14.6 | 3.7 | 3.0 | 27.80 | 28.05 | 3.2 | 3.0 |
| | 17.1 | 18.2 | 4.1 | 4.2 | 30.15 | 31.8 | 3.4 | 3.5 |
| | 18.9 | 18.9 | 4.5 | 4.5 | 30.15 | 25.82 | 3.6 | 3.2 |
| | 20.8 | 19.7 | 5.0 | 5.0 | 33.07 | 33.28 | 3.8 | 2.8 |
| | 22.9 | 22.1 | 5.5 | 5.5 | 34.02 | 33.95 | 3.8 | 3.8 |
| | 25.2 | 25.9 | 6.1 | 6.3 | 35.29 | 35.08 | 3.9 | 3.8 |
| | 30.5 | 31.1 | 7.4 | 7.7 | 35.80 | 36.82 | 3.9 | 3.6 |
| | 33.6 | 33.4 | 8.2 | 8.1 | 36.95 | 37.12 | 4.0 | 3.7 |
| Validate | 45.5 | 45.3 | 0.9 | 10.7 | 37.28 | 37.9 | 4.0 | 4.3 |
| | 8.7 | 10.0 | 2.0 | 2.5 | 25.54 | 25.08 | 3.2 | 3.0 |
| | 27.7 | 28.0 | 6.7 | 6.7 | 35.29 | 35.1 | 3.9 | 3.1 |
| Test | 37.5 | 36.8 | 9.0 | 8.6 | 35.80 | 36.08 | 3.9 | 3.8 |
| | 7.2 | 7.9 | 1.6 | 2.4 | 17.28 | 16.45 | 2.3 | 2.8 |
| | 14.1 | 13.9 | 3.3 | 2.9 | 33.07 | 33.25 | 3.8 | 3.6 |
| | 41.3 | 40.0 | 9.9 | 9.4 | 36.95 | 35.64 | 4.0 | 4.0 |

It can be noticed that, there are some repeated permittivity and conductivity values. This is because these values were used repeatedly for different transmitted and received UWB signals pair.

the decision would be that the tumor is malignant and immediate action has to be taken by doctors. If the values are in the range of 50–55, then urgent further medical diagnosis is needed to determine its type.

We could not generate tumors with permittivity and conductivity values greater than 38 and 4.0 (S/m) respectively. This is because the water-to-wheat flour mix would be so sticky that it cannot be handled easily. However, the principle is still valid and the system will be able

to detect and show any tumor types. Presently, we are preparing for clinical detection trial after obtaining the Ethical committee approval.

4. CONCLUSION

This paper proposes a NN-based UWB user friendly system to detect breast tumors in a 3D breast model. This system is trained by feature vectors obtained in 3D configuration. Differentiation between malignant and benign tumors based on dielectric properties is also achievable using the system setup. The accuracy of tumor existence detection is almost 100% for both simulation and experimental setup demonstrating the superiority of the experimental system. The achieved location detection accuracy are nearly 89.2% and 86.6% in simulation and experimental setups respectively. Tumor permittivity and conductivity prediction accuracy approximately 98% and 99.1% in simulation and 98.6% and 99.5% in experimental work respectively. This accuracy provides privilege to doctors to decide about the detected tumor type and take appropriate action in an early stage. The simulation work showed the first proof of using such a system, the experimental work provided the basis for actual clinical trials for tumor existence and its classification. Our next step (presently under investigation) is to include the tumor shape and growth in the NN training data to reduce the soft margin and increase detection reliability in terms of glandular tissue material.

REFERENCES

1. Lim, H. B., N. T. Nhung, E. Li, and N. D. Thang, "Confocal microwave imaging for breast cancer detection: Delay-multiply-and-sum image reconstruction algorithm," *IEEE Transactions on Biomedical Engineering*, Vol. 55, No. 6, 1697–1704, 2008.
2. Fear, E. C., X. Li, S. C. Hagness, and M. A. Stuchly, "Confocal microwave imaging for breast tumor detection: Localization of tumors in three dimensions," *IEEE Transactions on Biomedical Engineering*, Vol. 49, No. 8, 812–822, 2002.
3. O'Halloran, M., M. Glavin, and E. Jones, "Channel-ranked beamformer for the early detection of breast cancer," *Progress In Electromagnetic Research*, Vol. 103, 153–168, 2010.
4. Byrne, D., M. O'Halloran, M. Glavin, and E. Jones, "Data independent radar beamforming algorithms for breast cancer detection," *Progress In Electromagnetic Research*, Vol. 107, 331–348, 2010.

5. O'Halloran, M., M. Glavin, and E. Jones, "Rotating antenna microwave imaging system for breast cancer detection," *Progress In Electromagnetic Research*, Vol. 107, 203–217, 2010.
6. Alshehri, S. A. and S. Khatun, "UWB imaging for breast cancer detection using neural networks," *Progress In Electromagnetic Research C*, Vol. 7, 79–93, 2009.
7. Byrne, D., M. O'Halloran, E. Jones, and M. Glavin, "Transmitter-grouping robust capon beamforming for breast cancer detection," *Progress In Electromagnetic Research*, Vol. 108, 401–416, 2010.
8. Zhang, H., S. Y. Tan, and H. S. Tan, "A novel method for microwave breast cancer detection," *Progress In Electromagnetics Research*, Vol. 83, 413–434, 2008.
9. Bindu, G., A. Lonappan, V. Thomas, C. K. Ananadan, and K. T. Mathew, "Active microwave imaging for breast cancer detection," *Progress In Electromagnetic Research*, Vol. 58, 149–169, 2006.
10. Li, X., S. K. Davis, S. C. Hagness, D. W. Weide, and B. D. Veen, "Microwave imaging via space-time beam forming: Experimental investigation of tumor detection in multilayer breast phantoms," *IEEE Trans. Microwave Theory Techniques*, Vol. 52, No. 8, 1856–1865, 2004.
11. Klemm, M., I. Craddock, J. Leendertz, A. Preece, and R. Benjamin, "Radar-based breast cancer detection using a hemispherical antenna array — Experimental results," *IEEE Transactions on Antennas and Propagation*, Vol. 57, 1692–1704, 2009.
12. Lazaro, A., D. Girbau, and R. Villarino, "Simulated and experimental investigation of microwave imaging using UWB," *Progress In Electromagnetics Research*, Vol. 94, 263–280, 2009.
13. Lai, J. C., C. B. Soh, E. Gunawan, and K. S. Low, "Homogeneous and heterogeneous breast phantom for ultra-wideband microwave imaging applications," *Progress In Electromagnetic Research*, Vol. 100, 377–415, 2010.
14. Lazaro, A., D. Girbau, and R. Villarino, "Wavelet-based breast tumor localization technique using a UWB radar," *Progress In Electromagnetic Research*, Vol. 98, 75–95, 2009.
15. Alshehri, S. A., S. Khatun, A. Jantan, R. S. A. Raja Abdullah, R. Mahmud, and Z. Awang, "Experimental breast tumor detection using NN-based UWB imaging," *Progress In Electromagnetic Research*, Vol. 111, 447–465, 2011.
16. Sha, L., E. R. Ward, and B. Story, "A review of dielectric

- properties of normal and malignant breast tissue,” *Proceedings IEEE SoutheastCon*, 457–462, Apr. 5–7, 2002.
17. Lazebnik, M., et al., “A large-scale study of the ultrawideband microwave dielectric properties of normal, benign and malignant breast tissues obtained from cancer surgeries,” *Phys. Med. Biol.*, Vol. 52, 6093–6115, IOP Publishing, Oct. 2007.
 18. Rangayyan, R. M., N. M. El-Faramawy, J. E. Leo Desautels, and O. A. Alim, “Measures of acutance and shape for classification of breast tumor,” *IEEE Transactions on Medical Imaging*, Vol. 16, No. 6, Dec. 1997.
 19. Conceicao, R. C., M. O’Halloran, E. Jones, and M. Glavin, “Investigation of classifiers for early-stage breast cancer based on radar target signatures,” *Progress In Electromagnetic Research*, Vol. 105, 295–311, 2010.
 20. Davis, S. K., B. D. van Veen, S. C. Hagness, and F. Kelcz, “Breast tumor characterization based on ultrawideband microwave backscatter,” *IEEE Transactions on Biomedical Engineering*, Vol. 55, No. 1, Jan. 2008.
 21. Insana, M. F., C. Pellot-Barakat, M. Sridhar, and K. K. Lindfors, “Viscoelastic imaging of breast tumor microenvironment with ultrasound,” *Journal of Mammary Gland Biology and Neoplasia*, Vol. 9, No. 4, Oct. 2004.
 22. Bindu, G. and K. T. Mathew, “Characterization of benign and malignant breast tissues using 2-D microwave tomographic imaging,” *Microwave and Optical Technology Letters*, Vol. 49, No. 10, Oct. 2007.
 23. O’Halloran, M., B. McGinley, R. C. Conceicao, F. Morgan, E. Jones, and M. Glavin, “Spiking neural networks for breast cancer classification in a dielectrically heterogeneous breast,” *Progress In Electromagnetics Research*, Vol. 113, 413–428, 2011.
 24. Hagness, S. C., A. Taflove, and J. E. Bridges, “Three dimensional FDTD analysis of a pulsed microwave confocal system for breast cancer detection design of an antenna-array element,” *IEEE Transactions on Antennas and Propagation*, Vol. 47, No. 5, May 1999.
 25. CST Microwave Studio, CST Inc., 2009.
 26. Time Domain Corporation, Cummings Research Park, 330 Wynn Drive, Suite 300, Huntsville, AL 35805, USA.
 27. Dielectric Constants of Common Materials [http: //www.flowmeterdirectory.com/dielectric_constant_01.html](http://www.flowmeterdirectory.com/dielectric_constant_01.html).